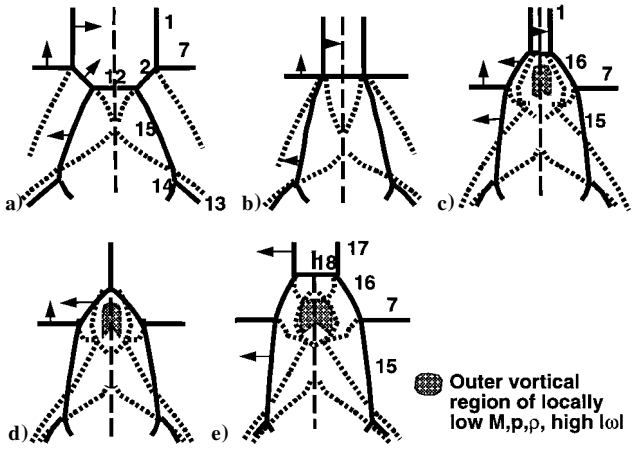

Fig. 4 Schematic representation of reflection of outer shock structure from symmetry plane. Not to scale.

The reflection of the corner shock 2 is relatively rapid and, as noted earlier, irregular. In Fig. 2f, the situation is depicted just before the reflection of the inviscid shock from the symmetry plane. The reflection of the corner shock is complete though the Mach stem (which may be associated with the transmitted ramp shock 18 introduced later) persists. In the final frame, Fig. 2g, the inviscid shock has also reflected off the symmetry plane. A plate centerline shock structure (PCS), which exists but is not so prominent in earlier frames, is also marked. This arises from an impingement of wall-jet-like features as described in Ref. 3.

The sequence of events between Figs. 2e and 2g is also intricate and is sketched in Fig. 4. Figure 4a depicts the features just before the termination of the corner shock 2. The reflection of the corner shock is complete in Fig. 4b. The inviscid shock approaches the symmetry plane in Fig. 4c, which is a schematic of Fig. 2f. A bridge shock 16 is formed, joining the fin inviscid, 1, and ramp embedded, 7, shocks. Slip lines emanate from each of the triple points, 1-12-16 and 7-15-16, as shown in Fig. 4d, where 1 reflects off the symmetry plane. The slip lines form a compact vortical region near the centerline characterized by locally low Mach number, density, and static pressure and high vorticity. The interior of this structure is difficult to discern with the present algorithm and is not detailed. However, the feature appears to be inviscid in origin because independent calculations with the Euler equations (not described here) also show similar development. In Fig. 4e, the inviscid shock has reflected off the symmetry plane to form 17: this situation is shown in Fig. 2f. A transmitted ramp shock, 18, is formed, whose effect is to account for the ramp deflection in the far downstream regions. In the experiment, this has been noted as a Mach stem. The ramp transmitted shock moves upward more rapidly than the ramp embedded shock 7. This follows from the fact that 7 deflects fluid that has previously been processed through 1 alone, whereas 18 processes the relatively lower Mach number fluid downstream of 1 as well as its reflection 17.

III. Conclusions

Computations have been utilized to investigate the shock structure in the multiple-shock/turbulent-boundary-layer interaction comprised by the triple-shock geometry. Near the ramp surface, there is significant similarity to symmetric DF interactions whose shock structure can be described in terms of the reflection of a λ shock from the symmetry plane. For this reason, near the surface, a commonality exists in the DF and TS flowfields in the principal coherent streamline features as has been shown in Ref. 4. The TS outer shock structure is, however, vastly more intricate. The various shock and slip surface components are augmented by an outer vortical structure, all of which are detailed with schematic interpretations.

Acknowledgments

This work was supported by the Air Force Office of Scientific Research sponsorship of Len Sakell and by a grant of computer time from the Department of Defense High Performance Computing Shared Resource Center, Corps of Engineers Waterways Experiment Station, Vicksburg, Mississippi.

References

[1]Garrison, T. J., Settles, G. S., and Horstman, C. C., "Measurements of the Triple Shock/Wave Turbulent Boundary-Layer Interaction," *AIAA Journal*, Vol. 34, No. 1, 1996, pp. 57–64.

[2]West, J. E., and Korkegi, R. H., "Supersonic Interaction in the Corner of Intersecting Wedges at High Reynolds Number," *AIAA Journal*, Vol. 10, No. 5, 1972, pp. 652–656.

[3]Gaitonde, D., and Shang, J. S., "The Structure of a Double-Fin Turbulent Interaction at Mach 4," *AIAA Journal*, Vol. 33, No. 12, 1995, pp. 2250–2258.

[4]Gaitonde, D. V., and Shang, J. S., "On 3-D Shock-Wave Turbulent Boundary Layer Interactions at Mach 4," AIAA Paper 96-0043, Jan. 1996.

A. D. Belegundu
Associate Editor

Fatigue Analysis of Cracked Aluminum Plates Repaired with Bonded Composite Patches

T. Y. Kam,* Y. C. Tsai,† K. H. Chu,† and J. H. Wu†
National Chiao Tung University,
Hsin Chu 300, Taiwan, Republic of China

I. Introduction

BONDED repair of aging structures with composite patches has been an important subject of research in recent years. Investigators have proposed various numerical techniques for stress analysis of repaired structures and the subsequent derivation of stress intensity factors.[1–10] A number of researchers have studied the fatigue behavior of cracked structures repaired with bonded composite patches.[11–13] For instance, Baker[12] studied the fatigue crack propagation of centrally cracked aluminum panels patched with boron/epoxy composites, and Leibovich et al.[13] investigated the effect of composite patches on the fatigue crack growth behavior of repaired parts. In previous work on fatigue behavior of repaired parts, effort has been devoted to the fatigue of repaired parts with center cracks. Though edge cracks developed in thin-wall type structural members are not uncommon, as yet not much work has been done in the fatigue of bonded repair of parts with edge cracks. In this Note, fatigue behavior of aluminum panels containing an edge crack repaired with bonded composite patches is studied. A method is proposed for determining stress intensity factor and fatigue life of the repaired structures. Strain at the crack tip obtained in the finite element analysis of the repaired structure is used to determine the stress intensity factor of the structure. The Paris law of crack propagation is used to predict fatigue life of the repaired structure. Fatigue tests of compact tension (C–T) specimens with and without bonded repairs under different environmental conditions are performed to validate the accuracy and feasibility of the proposed method.

II. Analytical Approach

Finite Element Model

The aluminum plate with an edge crack (Fig. 1) is symmetrically repaired with bonded composite patches. The patches are modeled as Mindlin plates and analyzed using eight-noded serendipity elements. The adhesive and the aluminum plate are modeled by three-dimensional brick elements of 20 nodes. The aspect ratio of the three-dimensional brick elements are chosen in such a way that no numerical instability will occur. Quarter-point elements are used to model the stress singularity condition at the crack tip. The compatibility conditions at the interfaces between the patch, adhesive, and cracked plate are observed in the finite element formulation. When studying crack propagation, perfect bonding at the interfaces

Received Sept. 30, 1996; revision received Sept. 6, 1997; accepted for publication Sept. 26, 1997.

*Professor, Department of Mechanical Engineering. Member AIAA.
†Graduate Student, Department of Mechanical Engineering.

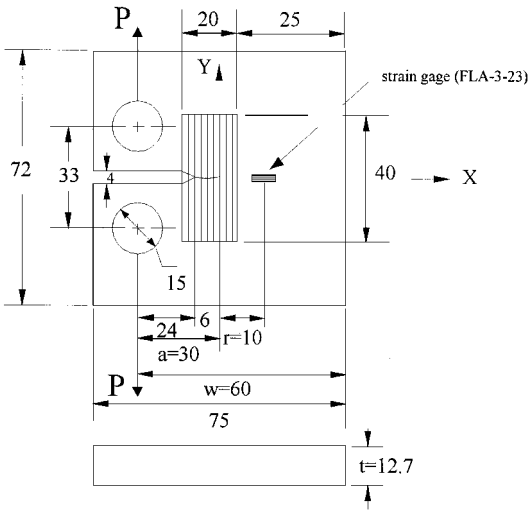

Fig. 1 Cracked C–T specimen repaired with bonded composite patch; units in millimeters.

is assumed and no debonding is considered in the finite element analysis of the repaired plate.

Stress Intensity Factor

According to Irwin,[14] the crack tip stress field of the cracked body in Fig. 1 subjected to symmetric (mode I) loading is given by

$$\begin{Bmatrix}\sigma_{xx}\\ \sigma_{yy}\\ \tau_{xy}\end{Bmatrix} = \frac{K_I}{\sqrt{2\pi r}}\cos\frac{\theta}{2}\begin{bmatrix}1-\sin\dfrac{\theta}{2}\sin\dfrac{3\theta}{2}\\ 1+\sin\dfrac{\theta}{2}\sin\dfrac{3\theta}{2}\\ \sin\dfrac{\theta}{2}\cos\dfrac{3\theta}{2}\end{bmatrix} \tag{1}$$

where σ_{ij} are stress components, K_I is the mode I stress intensity factor, r is the distance between the point of interest and the crack tip, and θ is the angle between r and the x axis.

It can be shown that, for the plane stress condition, the stress intensity factor can be expressed in terms of normal strain ε_{xx} at $\theta = 0$ near the crack tip:

$$K_I = \frac{\varepsilon_{xx} E\sqrt{2\pi r}}{1-\nu} \tag{2}$$

where E is Young's modulus and ν is Poisson's ratio. Once the normal strain ε_{xx} at a point along the x axis and near the crack tip has been determined in the finite element analysis, the stress intensity factor can then be calculated from Eq. (2).

Crack Propagation

The Paris law[15] of crack propagation is used to study the fatigue behaviors of cracked aluminum structures with and without repairs:

$$\frac{\mathrm{d}a}{\mathrm{d}N} = C(\Delta K)^m \tag{3}$$

where N is the number of the fatigue cycle; C, m are material constants; and ΔK is the difference between maximum and minimum values of the stress intensity factor during a fatigue cycle. The integration of Eq. (3) yields the fatigue life N_f of the cracked structure,

$$N_f = \int_{a_0}^{a_f} \frac{\mathrm{d}a}{C(\Delta K)^m} \tag{4}$$

where a_0 and a_f are initial and final crack lengths, respectively. The magnitude of ΔK depends on crack length. Thus, a series of finite element analyses of the cracked structure with different crack lengths is performed to trace the history of ΔK. Once the values of ΔK at different crack lengths are available, Eq. (4) is then solved via the numerical integration method using the Gauss rule to yield N_f. Factors such as residual thermal stresses induced by hot-cured adhesive for repaired structures and corrosion of metallic materials may have some effects on the value of C. Nevertheless, as will be shown in subsequent sections, these effects are small for the repaired structures considered in the present study. Therefore, it will be assumed that the value of C remains unchanged for the fatigue analysis of the cracked structures with or without repairs under different environmental conditions.

III. Experimental Approach

Fatigue tests of cracked aluminum C–T specimens repaired with bonded composite patches under different environmental conditions were performed to validate the analytical approach. The C–T specimens were made of 7075-T7351 aluminum and manufactured in accordance with American Society for Testing and Materials standards.[16] The composite patches were made of graphite/epoxy (Q-1115) prepreg tapes supplied by the Toho Company, Japan. The adhesive was composed of MB 1113 structure resin and 6726 base resin supplied by Narmco, United States. The properties of the C–T specimen, adhesive, and composite lamina are listed in Table 1. A number of C–T specimens without repair were first precracked to the size of $a \cong 30$ mm. The crack size was determined via visual inspection with the assistance of a microscope. Several of the precracked C–T specimens were then repaired symmetrically with bonded composite patches via the following cure cycle: temperature was 120°C, pressure was 40 psi, and curing time was 1 h. The dimensions of the repaired specimens are shown in Fig. 1.

Because both the thickness and the area of the patch are much smaller than those of the C–T specimen, it is reasonable to assume that the effect of residual thermal stresses induced by the hot-cured adhesive on the crack propagation of the specimen is small and, thus, can be neglected in the fatigue analysis. Specimens with and without repairs under normal environmental (noncorrosive) condition were subjected to cyclic load of mean 3300 N, amplitude 2700 N, and frequency 4 Hz via a 10-ton Instron testing machine. Matrix cracking was developed in the composite patches of thickness $h_p \leq 0.6$ mm when the repaired specimens were under fatigue. The fatigue life of the specimen without repair, N_q, was 23,545 cycles. The fatigue lives of the specimens repaired with patches of different thicknesses at $a = 40$ mm are listed in Table 2. Note that bonded composite repair is able to extend the fatigue life of cracked specimens in a significant way. In general, the increase in patch thickness can magnify the beneficial effect on the extension of fatigue life. The increase in fatigue life, however, slows down or even stops growing as the patch thickness reaches a certain value, for instance, 1.2 mm in the present study.

Several of the repaired specimens with patches of 0.6 mm thickness each were placed in a closed chamber filled with salty vapor. The weight ratio of salt to water was 1:200. The repaired specimens were stored in the closed chamber for different durations (0.5–2.0 months) before being subjected to fatigue tests. Inspection of the

Table 1 Properties of specimen and bonded composite patch

Aluminum	$t = 12.7$ mm, $E = 71.7$ GPa, $\nu = 0.33$, $C = 2.714 \times 10^{-8}$, $m = 3.158$
Adhesive	$E = 2.702$ GPa, $\nu = 0.4$, $t = 0.102$ mm
Graphite/epoxy ply	$E_1 = 132.5$ GPa, $E_2 = 7.9$ GPa, $G_{12} = 4.2$ GPa, $G_{23} = 1.02$ GPa, $\nu_{12} = 0.28$, $t = 0.15$ mm

Table 2 Fatigue lives of C–T specimens with repair

Thickness of patch, mm	0.3	0.6	0.9	1.2
Number of cycles	$6.8N_q$[a]	$8.7N_q$	$9.6N_q$	$9.7N_q$

[a] $N_q = 23{,}545$ cycles.

Table 3 Experimental stress intensity factors and fatigue lives of repaired specimen under different environmental conditions

Duration, months	K_I,[a] MPa$\sqrt{\text{m}}$	ΔK,[b] MPa$\sqrt{\text{m}}$	N_E, cycles
0	10.07	10.876	$8.7N_q$
0.5	10.30	11.124	$6.8N_q$
1.0	10.99	11.869	$5.6N_q$
2.0	12.16	13.133	$4.2N_q$

[a] $K_I = K_I(\bar{P})$. [b] $\Delta K = K_{I,\max}(P_{\max}) - K_{I,\min}(P_{\min})$.

specimens showed that each of them was covered with a thin layer of rust the thickness of which depended on the duration of the specimen having been in the corrosive environment. Because the corrosive layer is very thin (less than 0.5 mm) compared with the C–T specimen, its effect on the properties of the aluminum is assumed to be small and will not be considered in the fatigue analysis. On the contrary, the corrosive environment might have significant effects on the bonding properties of the adhesive. These effects could be reflected by the increase in stress intensity factor and the reduction in fatigue life of the repaired specimens. The repaired specimens removed from the environmental chamber were first subjected to static test and stress intensity factors at different load levels ($P = 3300$ N, $P_{\max} = 6000$ N, and $P_{\min} = 2700$ N); the stress intensity factors were determined from measured strains. The specimens were then subjected to fatigue tests and the lives of the specimens at $a = 40$ mm were recorded. The cyclic load was of mean 3300 N, amplitude 2700 N, and frequency 4 Hz. The stress intensity factors and fatigue lives of the specimens under different conditions are listed in Table 3. The corrosive environment did have significant effects on stress intensity factor and fatigue life of the repaired specimen as manifested in Table 3, i.e., longer duration in corrosive environment yielded a larger stress intensity factor as well as a shorter fatigue life. Nevertheless, note that even in the corrosive environment the fatigue life of the specimen with bonded repair was still longer than that of the specimen without repair.

IV. Results and Discussion

Stress Intensity Factor

The empirical equation for evaluating stress intensity factor of a C–T specimen without repair is expressed as [17]

$$K_I = \left(P/tW^{\frac{1}{2}}\right) f(\alpha) \tag{5a}$$

with

$$f(\alpha) = \frac{(2+\alpha)(0.886 + 4.64\alpha - 13.32\alpha^2 + 14.72\alpha^3 - 5.6\alpha^4)}{(1-\alpha)^{\frac{3}{2}}} \tag{5b}$$

where P is applied load, t is thickness of specimen, a is crack length, W is width of specimen, and $\alpha = a/W$. To verify the accuracy of the present approach, the stress intensity factor of the C–T specimen is also determined via the present finite element method. The NASTRAN finite element code[18] is adopted to perform the finite element analysis. The properties of the aluminum C–T specimen listed in Table 1 are used in the finite element analysis. Strains at different locations ahead of crack tip in the x direction obtained in the finite element analysis of the specimen are used to calculate the stress intensity factors from Eq. (2). The stress intensity factors determined from the empirical and the present finite element methods for $P = 5000$ N and $a = 30$ mm are listed in Table 4. The results obtained from the present finite element method match the empirical ones well if $10 \le r \le 15$ mm, where the differences between the two methods are less than 1%. The finite element method is then used to study the stress intensity factor of the C–T specimens repaired with bonded composite patches of different thicknesses. Strain ε_{xx} at $r = 10$ mm ahead of crack tip is used to determine the stress intensity factor of each repaired specimen. For purpose of comparison, strain at $r = 10$ mm ahead of crack tip was also measured experimentally, as shown in Fig. 1, and used to evaluate the stress intensity factor of each repaired specimen. The stress intensity factors obtained from the present method and the experiment are listed in Table 5. The finite element results closely match the experimental ones. That the stress intensity factors of the repaired specimens are much lower than those of the unrepaired ones demonstrates the advantage of repair with bonded composite patches. Note that the increase in patch thickness can reduce the stress intensity factor of the repaired specimen. The reduction in the stress intensity factor, however, may converge as the patch thickness increases to some particular value.

The present method is also used to determine stress intensity factors of different crack lengths. Figure 2 shows the stress intensity factors of different crack lengths for the specimens with and without repairs. The stress intensity factor of the repaired specimen varies only slightly with respect to crack length, whereas that of the unrepaired specimen increases monotonically as the crack length increases.

Table 4 Stress intensity factors of unrepaired C–T specimens obtained by different methods

		Finite element (II)			
Method	Empirical (I)	$r = 10$ mm	$r = 15$ mm	$r = 20$ mm	$r = 25$ mm
K_I, MPa $\sqrt{\text{m}}$	15.525	15.39	15.40	13.84	16.45
Difference $\lvert(\text{II} - \text{I})/\text{I}\rvert$%	——	0.87	0.81	10.8	5.9

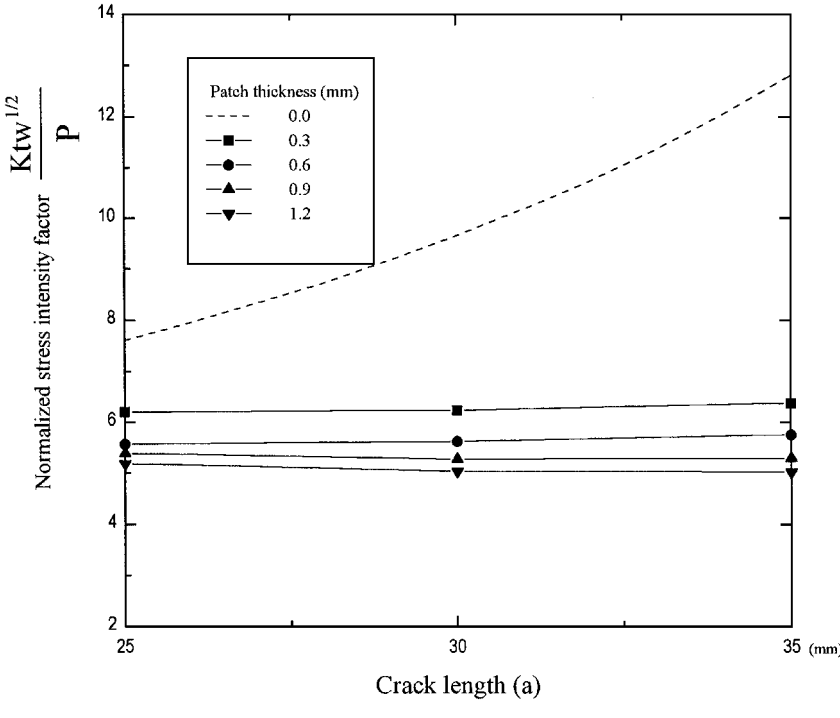

Fig. 2 Stress intensity factors of C–T specimens repaired with bonded composite patches of different thicknesses.

Table 5 Stress intensity factors of repaired C–T specimens with crack size $a = 30$ mm

Thickness of patch, mm	Finite element (I) K_{Ir}/K_I[a]	Experiment (II) K_{Ir}/K_I	Difference $\lvert(\text{II} - \text{I})/\text{II}\rvert\%$
0.3	0.695	0.689	0.87
0.6	0.676	0.648	4.32
0.9	0.573	0.613	6.52
1.2	0.566	0.610	7.21

[a] K_I is stress intensity factor of unrepaired specimen (15.525 MPa$\sqrt{\text{m}}$) and K_{Ir} is stress intensity factor of repaired specimen.

Table 6 Theoretical fatigue lives of repaired specimens

Thickness of patch, mm	0.3	0.6	0.9	1.2
Fatigue life N_T, cycles	$7.0N_q$	$8.5N_q$	$10.2N_q$	$10.3N_q$
Difference[a] $\lvert(N_E - N_T)/N_E\rvert\%$	3.00	2.30	6.25	6.20

[a] N_E is experimental fatigue life.

Table 7 Theoretically predicted fatigue lives of repaired specimens in corrosive environment for different durations

Duration, month	Predicted life N_T, cycles	Difference[a] $\lvert(N_T - N_E)/N_E\rvert\%$
0.5	$7.9N_q$	9.2
1	$6.4N_q$	6.9
2	$4.7N_q$	12.0

[a] N_E are experimental fatigue lives from Table 3.

Fatigue Life Estimation

The information on stress intensity factors of different crack lengths, which is obtained from a series of finite element analyses of repaired C–T specimens with different crack lengths, is used in Eq. (4) to yield the fatigue lives of the repaired specimens. The initial and final crack lengths are set as 30 and 40 mm, respectively. The properties of the composite patch listed in Table 1 are used in the fatigue study. The theoretically predicted fatigue lives of the repaired specimens are listed in Table 6. When comparing the theoretical fatigue lives in Table 6 with the experimental ones in Table 2, it is found that their differences are less than 6.3%, as indicated in Table 6. This demonstrates that the use of the present method for stress intensity factor evaluation and the use of the Paris law for fatigue life prediction of cracked aluminum specimens repaired with bonded composite patches are feasible and yield good results.

The Paris law is also used to study the fatigue life of the repaired specimens subject to a corrosive environment. The measured ΔK (difference of stress intensity factors) at $a = 30$ mm were used in the prediction of fatigue life. In view of the slight variation of stress intensity factor with respect to crack length for the repaired specimens in a normal environment, it is assumed that the difference of stress intensity factors of the repaired specimens in a corrosive environment is independent of crack length. Because the durations of the repaired specimens in corrosive environment are short and the environmental effects on constants C and m are small, it is assumed that the values for C and m in Table 1 can still be used in the fatigue analysis of the specimens. Environmental effects on the properties of the adhesive have been implicitly included in the magnitudes of the measured stress intensity factors. Using the measured ΔK, the theoretical fatigue lives of the repaired specimens are determined from Eq. (4). Comparisons between theoretical and experimental fatigue lives are made, and the differences are less than or equal to 12%, as given in Table 7.

V. Conclusion

A method for fatigue life estimation of cracked aluminum plates repaired with bonded composite patches was proposed. Stress analysis was accomplished via the finite element method, and the stress intensity factor was determined via a strain approach. The Paris law was used to estimate the fatigue lives of the cracked plates with and without bonded repairs. Experiments were performed to study stress intensity factor and fatigue life of aluminum C–T specimens repaired with bonded composite patches under different environmental conditions. Experimental results were used to validate the accuracy and feasibility of the proposed method. It has been demonstrated that the present method is able to yield good predictions of stress intensity factor and fatigue life of cracked plates repaired with bonded composite patches. Double-sided repair has beneficial effects on the extension of fatigue life of plates with edge cracks under different environmental conditions. Nevertheless, there exists an optimum patch thickness beyond which the beneficial effects stop growing. Furthermore, the beneficial effects for repaired specimens diminish as the duration in corrosive environment increases. Should the effects induced by adhesive debonding or degradation, residual thermal stresses, and corrosion be considered in the fatigue analysis of the repaired specimens, much better theoretical predictions may be obtained as expected.

Acknowledgment

This research was supported by the National Science Council of the Republic of China under Grant NSC 85-2212-E-009-016. Their support is gratefully acknowledged.

References

[1]Baker, A. A., and Jones, R., *Bonded Repair of Aircraft Structure*, Martinus–Nijhoff, Dordrecht, The Netherlands, 1988, pp. 1–214.

[2]Young, A., Cartwright, D. J., and Rooke, D. P., "The Boundary Element Method for Analyzing Repair Patches on Cracked Finite Sheets," *Aeronautical Journal of the Royal Aeronautical Society*, Dec. 1988, pp. 416–421.

[3]Young, A., Cartwright, D. J., and Rooke, D. P., "Analysis of Patched and Stiffened Cracked Panels Using the Boundary Element Method," *International Journal of Solids and Structures*, Vol. 29, No. 17, 1992, pp. 2201–2216.

[4]Park, J. H., Ogiso, T., and Atluri, S. N., "Analysis of Crack in Aging Aircraft Structures with and without Composite-Patch Repairs," *Computational Mechanics*, Vol. 10, Nos. 3/4, 1992, pp. 169–201.

[5]Young, A., Rooke, D. P., and Cartwright, D. J., "Numerical Study of Balanced Patch Repairs to Cracked Sheets," *Aeronautical Journal of the Royal Aeronautical Society*, Vol. 93, Nov. 1989, pp. 327–333.

[6]Sun, C. T., Klug, J., and Arendt, C., "Analysis of Cracked Aluminum Plates Repaired with Bonded Composite Patches," *AIAA Journal*, Vol. 34, No. 2, 1996, pp. 369–374.

[7]Chue, C. H., Chang, L. C., and Tsai, J. S., "Bonded Repair of a Plate with Inclined Central Crack Under Biaxial Loading," *Composite Structures*, Vol. 28, No. 1, 1994, pp. 39–45.

[8]Sethuraman, R., and Maiti, S. K., "Finite Element Analysis of Doubly Bonded Crack-Stiffened Panels Under Mode I or Mode II Loading," *Engineering Fracture Mechanics*, Vol. 34, No. 2, 1989, pp. 465–475.

[9]Alawi, H., and Saleh, I. E., "Fatigue Crack Growth Retardation by Bonding Patches," *Engineering Fracture Mechanics*, Vol. 42, No. 5, 1992, pp. 861–868.

[10]Lin, C. C., Chu, R. C., and Lin, Y. S., "A Finite Element Model for Single-Sided Crack Patchings," *Engineering Fracture Mechanics*, Vol. 46, No. 6, 1993, pp. 1005–1021.

[11]Ratwani, M. M., "Characterization of Fatigue Crack Growth in Bonded Structures," U.S. Air Force Flight Dynamics Lab., Rept. AFFDL-TR-77-31, Vols. 1 and 2, Wright–Patterson AFB, OH, June 1977.

[12]Baker, A. A., "Fatigue Crack Propagation Studies on Aluminum Panels Patched with Boron/Epoxy Composite," *International Conference on Aircraft Damage Assessment and Repair* (Melbourne, Australia), edited by R. Jones and N. J. Miller, Inst. of Engineers, 1991, pp. 209–215.

[13]Leibovich, H., Sasson, N., Simon, A., and Green, A. K., "Repair of Cracked Aluminum Aircraft Structure with Graphite/Epoxy Patches," *Proceedings of the 9th International Conference on Composite Materials* (Madrid, Spain), edited by A. Miravete, Vol. 4, Woodhead, Cambridge, England, UK, 1993, pp. 461–468.

[14]Irwin, G. R., "Analysis of Stresses and Strains near the end of a Crack Traversing a Plate," *Journal of Applied Mechanics*, Vol. 24, No. 3, 1957, pp. 361–364.

[15]Broek, D., *Elementary Engineering Fracture Mechanics*, Noordhoff International, Leyden, The Netherlands, 1974.

[16]"Constant-Load-Amplitude Fatigue Crack Growth Rates Above 10^{-8} m/cycle," Annual American Society for Testing and Materials Standard, E647-78T, Ann Arbor Press, Ann Arbor, MI, 1978.

[17]Anderson, T. L., *Fracture Mechanics*, CRC Press, New York, 1995, pp. 712, 713.

[18]"MSC/NASTRAN Version 66," MacNeal–Schwendler Corp., Los Angeles, CA, 1990.

G. A. Kardomateas
Associate Editor